Mon. Not. R. Astron. Soc. **336,** 119–130 (2002)

Tidal debris of dwarf spheroidals as a probe of structure formation models

Lucio Mayer,[1⋆] Ben Moore,[2⋆] Thomas Quinn,[1⋆] Fabio Governato[1,3⋆] and Joachim Stadel[4⋆]

[1] *Department of Astronomy, University of Washington, Seattle, WA 98195, USA*
[2] *Institute for Theoretical Physics, University of Zürich, Winterthurerstrasse 190, CH-8057 Zürich, Switzerland*
[3] *Osservatorio Astronomico di Brera, via Bianchi 46, I-23807 Merate (LC), Italy*
[4] *University of Victoria, Department of Physics and Astronomy, 3800 Finnerty Road, Elliot Building, Victoria, BC, V8W 3PG Canada*

Accepted 2002 May 27. Received 2002 May 22; in original form 2001 October 19

ABSTRACT

Recent observations suggest that Carina and other nearby dwarf spheroidal galaxies (dSphs) are surrounded by unbound stars tidally stripped by the Milky Way. We have run high-resolution *N*-body simulations of dwarf galaxies orbiting within the Milky Way halo to determine if such observations can be explained with dark matter potentials like those implied by current structure formation models. We show that tidal forces acting on dwarfs with constant density cores or with cuspy profiles having a low concentration parameter ($c \lesssim 7$) lead to flat outer stellar density profiles like that of Carina for a variety of orbital configurations. On the contrary, it is more difficult to remove stars from cuspy dark matter haloes with concentrations as high as predicted by cold dark matter (CDM) models at the mass scale of dwarf galaxies ($c > 10$), and the data can only be reproduced assuming nearly radial orbits. Our simulations show that Carina is losing mass at a fractional rate <0.1 Gyr^{-1} and its mass-to-light ratio could be inflated by at most a factor of 2 due to unbound stars projected along the line of sight. We follow the evolution of the tidal debris within a triaxial clumpy cold dark matter Milky Way halo which causes differential precession and small-scale heating of the stellar streams. This renders them useless as a dynamical tracer of the Galactic potential in CDM cosmogonies. Models with warm dark matter (WDM) or collisional fluid dark matter (FDM) produce dwarf haloes with lower central densities than CDM and would be consistent with the observed tidal tails even for orbits with eccentricities as low as indicated by current data on nearby dwarf spheroidals. Galactic haloes in models with FDM are expected to be smooth and spherical and would be favoured by the detection of cold coherent streams such as that associated with the Sagittarius dwarf spheroidal. In this respect the distribution of stellar streams on the plane of the sky can provide a novel test of the nature of the dark matter. On the other end, the streams could be similarly dispersed in lumpy CDM haloes and in smoother, triaxial WDM haloes.

Key words: methods: *N*-body simulations – galaxies: dwarf – galaxies: evolution – galaxies: interactions – Local Group – dark matter.

1 INTRODUCTION

In hierarchical models of structure formation, the first dark matter clumps that eventually host luminous galaxies have masses comparable to the smallest dwarf galaxies in the Local Group (Haiman, Thoul & Loeb 1996a; Haiman, Rees & Loeb 1996b; Tegmark et al. 1997). In these models, dwarf galaxies represent the cornerstones of galaxy formation; observations of dwarf galaxies should thus provide fundamental tests to our current understanding of how structure formation has proceeded in the Universe. Some of the properties of dwarf galaxy populations in the Local Group and other nearby groups (Grebel 1999, 2001) can be understood within the hierarchical clustering scenario. The morphology–density relation, namely the fact that dwarf spheroidals (dSphs) are clustered around the dominant galaxies in the groups, while the dwarf irregulars (dIrrs) are found at much larger distances from them (Mateo 1998; Grebel 2001), probably reflects the continuous transformation of dIrrs into

⋆E-mail: mayer@astro.washington.edu (LM); moore@physik.unizh.ch (BM); trq@astro.washington.edu (TQ); fabio@merate.mi.astro.it (FG); stadel@phys.uvic.ca (JS)

dSphs as they fall into the overdensity of the group and are stirred by the tidal field of the primary galaxies (Mayer et al. 2001a,b). On the other hand, the currently popular incarnations of hierarchical scenarios, namely cold dark matter (CDM) models, are challenged by the apparent dearth of small satellites below $V_c = 30\,\mathrm{km\,s^{-1}}$ (Klypin et al. 1999; Moore et al. 1999a) and by the rotation curves of dIrrs and low surface brightness (LSB) galaxies, which suggest that their haloes have constant-density cores (Lake & Skillman 1989; Cote, Freeman & Carignan 1997; de Blok & McGaugh 1997; van den Bosch et al. 2000; de Blok et al. 2001; McGaugh, Rubin & de Blok 2001) instead of the steep cusps found in numerical simulations of structure formation (Navarro, Frenk & White 1996, 1997; Moore et al. 1999a; Ghigna et al. 2000; Jing & Suto 2000; Power et al. 2002). These problems have recently motivated the exploration of alternative models, such as self-interacting dark matter (SIDM; Spergel & Steinhardt 2000; Moore et al. 2000; Yoshida et al. 2000a,b; Firmani et al. 2000), warm dark matter (WDM; Bode, Ostriker & Turok 2001; Dalcanton & Hogan 2001; Avila-Reese et al. 2001) and fluid dark matter (FDM; Peebles & Vilenkin 1999; Peebles 2000).

Dwarf spheroidal galaxies in the Local Group are the faintest galaxies known in the Universe to date ($M_B > -12$) and, in the traditional view, their large velocity dispersions reflect high dark matter contents (Mateo 1998). The long-lasting tidal interaction with the Milky Way and M31 should strip stars and dark matter from their potentials, leading to the formation of stellar and dark matter streams orbiting within the halo of the primaries (Ibata & Lewis 1998; Johnston, Sigurdsson & Hernquist 1998; Helmi & White 1999). Observational evidence of streams associated with tidally stripped dwarfs, such as Sagittarius, is constantly accumulating in the stellar halo of the Milky Way (Helmi et al. 1989, 2001; Ivezic et al. 2000; Martinez-Delgado et al. 2001b; Ibata et al. 2001a; Dohm-Palmer et al. 2001; Vivas et al. 2001) and, more recently, even around the nearby Andromeda galaxy (Ibata et al. 2001b). For more distant dSphs, the flattening of the star counts in the vicinity of the nominal tidal radius (Irwin & Hatzidimitriou 1995) has often been interpreted as a signature of the presence of tidal tails (Johnston et al. 1998). However, some authors have argued that such peculiar profiles indicate that the dwarfs are not bound and thus no dark matter would be needed to explain the large velocity dispersions (Kuhn & Miller 1989; Kuhn 1993; Klessen & Kroupa 1998). Recently, observations that take advantage of wide-field photometry have confirmed the flattening of the star counts out to larger radii in Carina (Majewski et al. 2000), while the cases of Draco (Piatek et al. 2001) and Ursa Minor (Martinez-Delgado et al. 2001a) are still controversial. Majewski et al. claim, on the basis of the observed extratidal extension, that Carina must have experienced a very large mass-loss rate, losing more than 90 per cent of its initial mass in 10 Gyr as a result of stripping by the Milky Way's tides.

The size and mass of unbound structures originating from the galaxies must be determined by both the typical densities of the latter (including dark matter) and the scalelength of their stellar components. Very dense systems, or systems with stellar components whose size is such that they lie well inside the tidal radius, will be harder to strip (Moore, Katz & Lake 1996). In CDM models, dark matter haloes have cuspy profiles with inner slopes $\sim r^{-1}$ or steeper (Dubinski & Carlberg 1991; Navarro et al. 1997; Moore et al. 1999b; Ghigna et al. 2000), but their typical densities within the radius of the stellar component, measured by the concentration $c = r_t/r_s$ (where r_s is the characteristic scale radius and r_t is the tidal radius), can vary considerably (Bullock et al. 2001); the higher the concentration, the steeper is the rise of the rotation curve and hence the local escape speed will also be higher.

It has been shown that there is enough freedom in the structural parameters allowed by CDM for large galaxies in the process of merging to form massive tails as observed (Dubinski, Mihos & Hernquist 1996; Mihos, Dubinski & Hernquist 1998; Springel & White 1999). However, these conclusions cannot be trivially extended to smaller mass scales because the typical concentration of haloes (and thus their central density) increases substantially with decreasing mass in CDM cosmogonies (Navarro et al. 1997). Moreover, the choice of the orbital parameters of the interacting systems also plays a role by defining both the typical intensity and the time dependence of the external tidal forces; for the dwarf satellites of the Milky Way and M31, we have distances and some information on the orbits themselves (Mateo 1998), which allows us to constrain the parameter space better than in the case of more remote binary systems. In addition, the subsequent evolution of the material stripped from dwarf satellites can provide useful information on the potential of the Milky Way and M31; in fact, the orbits that the tidal debris will follow will reflect the underlying mass distribution.

In order to explore the role of tidal effects on stellar systems embedded in haloes analogous to those forming in cold dark matter models, we have carried out several high-resolution *N*-body simulations of dwarf galaxies interacting with the external potential of the Milky Way. The simulations were performed with PKDGRAV, a fast, parallel binary tree code (Dikaiakos & Stadel 1996; Stadel, Quinn & Wadsley, in preparation). This paper is organized as follows: in the next section we will provide a description of the models used for the dwarf galaxies, Section 3 will be devoted to the results of the simulation, and finally we will discuss and summarize our findings.

2 INITIAL CONDITIONS

Many previous studies that investigated the tidal disruption of dSphs (Ibata & Lewis 1998; Johnston et al. 1998; Klessen & Kroupa 1998; Helmi & White 1999) employed spherical King models to represent their mass distribution and placed them on circular or nearly circular orbits in the potential of the primary halo. The structure and orbits of the galaxies were thus detached from the predictions of structure formation models. We use more sophisticated models of dwarf satellites, whose halo masses, sizes and density profiles are consistent with those of objects already in place at $z = 1$ in hierarchical cosmologies (White & Frenk 1991), the dSphs being at least as old (Mateo 1998). The initial dwarf models are placed on bound orbits in the Milky Way halo, which is modelled by the external potential of an isothermal sphere with mass $M_{\mathrm{prim}} \simeq 3 \times 10^{12}\,\mathrm{M_\odot}$, circular velocity $V_{\mathrm{prim}} = 220\,\mathrm{km\,s^{-1}}$, virial radius $R_{\mathrm{prim}} = 400$ kpc and core radius of 4 kpc (see Mayer et al. 2001b, for more details). The dwarfs are rotationally supported, exponential discs embedded in isothermal haloes with a core or NFW haloes (Hernquist 1993; Springel & White 1999) and resemble observed dIrrs. Discs and haloes are sampled by 5×10^4 and 3.5×10^5 particles, respectively. After several orbits the dwarfs will be transformed into dSphs and will satisfy the morphology–density relation (Mayer et al. 2001a,b).

The haloes are exponentially truncated at $r_t = R_{200}$, where R_{200} is their virial radius, namely the radius encompassing an overdensity equivalent to 200 times the average density of the Universe (White & Frenk 1991). In particular, here we consider models of LSB dIrrs because these are the likely progenitors of dSphs (Mayer et al. 2001a,b). The models with truncated isothermal haloes have a

constant-density core with radius r_c such that $r_c = 0.035 r_t$. Models with NFW haloes are characterized by the concentration $c = r_t/r_s$, where r_s is the characteristic scalelength of the halo, namely the radius at which the slope of the profile changes from r^{-3} to r^{-1} (Navarro et al. 1996, 1997); we consider models with $c = 4$, 7 or 12. The satellites span a range in initial circular velocities, from $V_c = 25$ to 75 km s^{-1}, corresponding to masses between 10^9 and 10^{11} $M_\odot$; in this mass range typically $c \geqslant 10$ in LCDM models, with $c = 12$ being actually a lower limit for the least massive among our satellite models (Eke, Navarro & Steinmetz 2001; Bullock et al. 2001). The surface density of the discs is kept fixed (except in model LIs3 and in the model described in Section 4.1) and corresponds to a central (B-band) surface brightness $\mu_B \sim 23.5$ mag arcsec^{-2} assuming a stellar mass-to-light ratio $(M/L_B)_\star = 2$ (Bottema 1997; de Blok & McGaugh 1997). Models of different masses are simply rescaled using the cosmological scaling between virial mass, virial radius and circular velocity (Mo, Mao & White 1998). The details of the procedure used to assign the structural parameters of the halo and discs of the satellites are explained in Mayer et al. (2001a,b).

The models employed in this paper include a major improvement in that the scalelength of the discs, r_h, instead of being a free parameter, is determined by the structural parameters of the dark halo, as in current galaxy formation models (Mo et al. 1998). In the latter models it is assumed that the specific angular momentum of the gas bound to the dark halo that cools and eventually falls towards the centre, forming the stellar disc, is initially equal to that of the halo and is conserved during such infall (Fall & Efstathiou 1980). In the simplest case in which the dark matter halo is a singular isothermal sphere and the response of the halo to the collapse of baryons is neglected, we have $r_h = 1/\sqrt{2}\lambda R_{200}$, where λ is the spin parameter, which measures the amount of kinetic energy of the halo stored into rotation, $\lambda = J|E|^{1/2}/GM^{5/2}$ (M is the halo mass, E is its binding energy and J is its total angular momentum). N-body simulations show that the spin parameter of large samples of haloes follows a log-normal distribution, with mean values in the range $0.035 \leqslant \lambda \leqslant 0.05$ and dispersions $\sigma_\lambda \sim 0.6$ (Barnes & Efstathiou 1987; Warren et al. 1992; Gardner 2001). Many of the models considered here have more realistic NFW profiles and the scalelength of the discs depends not only on λ but also on the concentration c and on the halo/disc mass ratio (see Springel & White 1999). Indeed, a higher concentration results in a smaller scalelength because the potential well of the halo is deeper and the disc needs to contract more to be in centrifugal equilibrium; in addition, the more baryonic mass that accumulates at the centre, the more the halo adiabatically contracts in response, making the potential well even deeper and reducing even further the final scalelength of the baryons (however, the halo/disc mass ratio is always close to $\sim$50 in all our models).

Our reference isothermal LSB models (LIs1, see Fig. 1) have scalelengths corresponding to $\lambda = 0.065$ (i.e. slightly above the average values); the resulting scalelength is equal to the core radius of the halo, this being consistent with the analysis of rotation curves in the sample of dIrrs/LSB galaxies in de Blok & McGaugh (1997). We also consider a model with the same r_c but r_h lowered by a factor of 2, which corresponds to a smaller spin parameter, $\lambda = 0.035$ (model LIs3 in Fig. 1); this model has the same disc mass as model LIs1, and thus the central surface brightness is $\mu_B \sim 22$ mag arcsec^{-2} (1.5 mag higher than the standard value). The reference NFW model with $c = 7$ and $\lambda = 0.065$ (model LNc7s1 in Fig. 1) has the same disc mass and radius as the isothermal model LIs1 but the rotation curve rises more steeply; the rotation curve of the isothermal model is better reproduced by a model with $c = 4$ (model LNc4s1 in Fig. 1). We also build models having different values of λ at fixed c; models

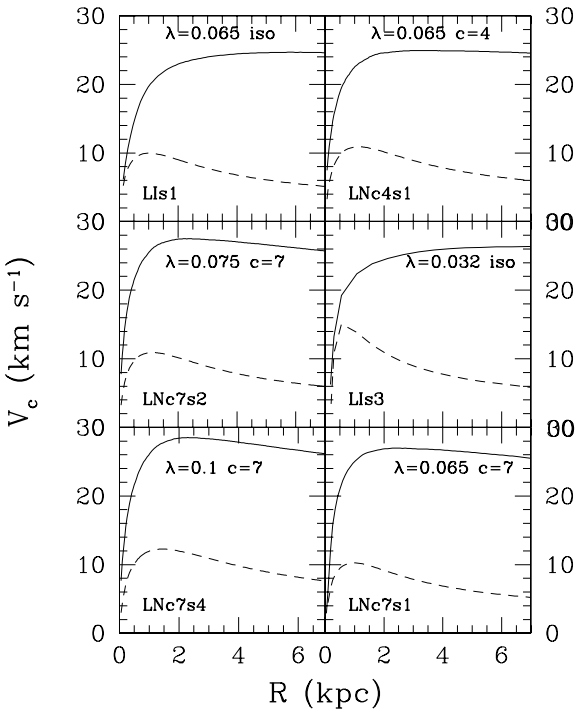

Figure 1. Rotation curves of initial model galaxies for the smallest mass scale considered ($V_c = 25$ km s^{-1}, $M_{sat} = 3 \times 10^{-4}$ M_{prim}). The other mass models are simply rescaled versions of those shown here, as explained in the text. In the panels the spin λ and concentration c (the latter only for the satellites with NFW haloes) are indicated. We recall that the isothermal models have a fixed core radius $r_c = 0.035 r_t$, while the disc scalelength varies according to λ. The related model names (used throughout the text) are in the bottom left corner of each panel.

LNc7s2 and LNc7s4 have $c = 7$ but $\lambda = 0.075$ and 0.1, respectively (a value of λ as high as 0.1 is found in $\lesssim$30 per cent of haloes in cosmological simulations). Finally, we build a model with $c = 12$ for the case of the largest value of the spin parameter ($\lambda = 0.1$), model LNc12s4.

We consider different orbital eccentricities, ranging from apo/peri = 2 to 15, and different disc orientations, although we neglect cases in which the satellites are on retrograde orbits, as it is well known that this configuration strongly inhibits the formation of tidal tails, irrespective of the internal structure of galaxies (Toomre & Toomre 1972; Dubinski et al. 1996; Springel & White 1999; Mayer et al. 2001a,b). The orbits have apocentres between 150 and 250 kpc and pericentres between 20 and 80 kpc, thus encompassing the whole range of galactocentric distances of dSphs.

3 RESULTS

Here we present the results of the simulations in three separate subsections. In Section 3.1 we will show that we are able to reproduce the observed outer flat profile of Carina, and that this happens when the halo of the dwarf has a sufficiently shallow mass distribution or when the orbit is nearly radial. In Section 3.2 we will measure the stellar mass-loss rates of satellites in our simulations and we will attempt to explain such results using simple dynamical arguments. Finally, in Section 3.3 we will evolve the tidal debris of spherical dwarf models within a CDM halo extracted from a cosmological simulation and will show how the streams undergo precession and

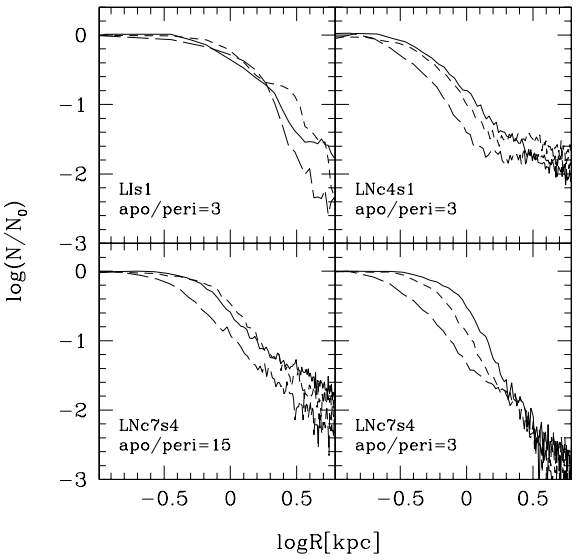

Figure 2. Projected star counts (after 7 Gyr) for representative remnants whose haloes all have the same circular velocity, $V_c = 25$ km s^{-1}, corresponding to an initial total mass $M_{sat} \sim 10^{-4}\ M_{prim}$, where M_{prim} is the mass of the primary halo. In each panel we show the projected star counts obtained observing the stars along one of the tails (solid line) and along the two lines of sight perpendicular to the former (short dashed and long dashed lines). The names of the models employed and the orbital eccentricities are also indicated in the panels (the apocentre of the orbits is fixed at $R_{apo} =$ 270 kpc, so the pericentre is as small as 18 kpc in the case of the most eccentric orbit). (See Fig. 1 for the corresponding structural parameters.)

heating by substructure, losing their coherence and becoming difficult to detect.

3.1 Tidal features and the internal structure of satellites

The satellites are severely stripped by the Milky Way tides but a bound stellar and dark component survives until the end of the simulations ($\lesssim$10 Gyr); after a few orbits (the orbital times are of the order of 2–3 Gyr), the stellar disc is transformed into a moderately triaxial system supported by velocity dispersion that closely resembles a dSph (see also Mayer et al. 2001a,b). Fig. 2 shows the final projected star counts from four representative simulations. In all cases we find tidal streams of stars escaping from the satellites which show up as a flattening of the outer projected star counts. The surface brightness of the tails depends strongly on the orbit and the structure of the initial models; the 'strength' of the streams can be quantified simply by the ratio of the star counts where the profile starts to flatten out (the so-called 'break radius'; see Johnston et al. (1999) relative to the counts at the centre of the dwarf, N_s/N_0. Satellites with cored isothermal haloes or low-concentration ($c = 4$) NFW haloes have $N_s/N_0 \approx 10^{-2}$ on orbits with moderate eccentricities (apo/peri = 2–3) and should reproduce the extended flattened star counts observed in Carina (Majewski et al. 2000). Instead, the streams are much weaker and would hardly match the observations when the concentration is almost doubled ($c = 7$), unless the orbits are nearly radial (Fig. 2). In this case $N_s/N_0 \gtrsim 10^{-3}$.

Indeed, raising the concentration by a factor of 2 leads to an increase of nearly 30 per cent in the escape speed at the half-mass radius of the stellar component, where the rotation curve peaks (This also increases their robustness to tides since the response of the system will be more adiabatic – see Section 3.2.). This is true even when the satellite is constructed with λ considerably larger than the mean and thus acquires a larger disc scalelength (as in the model LNc7s4 shown in Fig. 2). Therefore the value of the concentration is the most important parameter in determining the amount of stripped material; in fact, while a change in the spin affects only the disc scalelength, a change in the concentration affects both the scalelength and the central density of the halo, or, equivalently, its local escape speed. However, if the initial disc scalelength is substantially decreased while keeping the disc mass fixed, the resulting higher surface density of the disc can have a substantial impact on its evolution by enhancing the non-axisymmetric instabilities that drive the morphological transformation; for example, in model LIs3, the high self-gravity of the compact disc leads to a bar instability stronger than in the other cases and later to a very compact stellar remnant, thereby inhibiting the developing of tidal tails even if the halo has a fairly large core (see also Mayer et al. 2001b).

The simulations show that the visible strength of tidal extensions is sensitive to projection effects (Fig. 2). The results by Majewski et al. (2000) show a strong flattening of the star counts at a distance comparable to the tidal radius of the dwarf galaxy, where the counts level out at $\sim 10^{-2}$ times the peak value. In our models the slope of the star counts profile becomes shallower at smaller radii and at a higher N_s/N_0 when the line of sight of the observer falls *along* one of the tidal tails, because the projected surface density of the tails is maximally enhanced in this case and thus the contamination of the intrinsic profile of the dwarf is higher. When viewed perpendicular to the orbit, the profile becomes shallower at larger distance from the centre, but the change of slope is more drastic as the bound and unbound stellar components overlap less; in this case the tails would be distinguished more easily from the bound galaxy but they would have the lowest surface density (indeed corresponding to the actual intrinsic value), $\mu_B > 30$ mag arcsec^{-2}.

In Fig. 3 we show a more quantitative comparison between the results of the simulations and the star counts of Carina derived by Majewski et al. (2000) for satellites placed on a low-eccentricity orbit (apo/peri = 3). We plot the star counts for a line of sight falling along one of the tidal tails, chosen in order to have an upper limit on the outer flattening of the profile and thereby exclude satellite models whose star count profiles fall below the data. All the models have initially $V_c = 25$ km s^{-1}, corresponding to the smallest mass scale considered in this paper (the initial total mass is only 5.8×10^8 M$_\odot$). Starting with such a small initial mass, the satellites have physical scales close to those of Carina by the end of the simulations (after 7–8 Gyr). Indeed, the core radius of the bound remnant estimated from the fit with a King model with $c = 0.5$ is around 500 pc, the luminosity of the remnants is $M_B \sim -11$, assuming a final stellar mass-to-light ratio of 5 [as derived by combining population synthesis models with a model for the star formation history as described in Mayer et al. (2001a)]. Also, the final dark matter mass is almost five times higher than the stellar mass, yielding a central velocity dispersion $\sim$10 km s^{-1}, as seen in Fig. 4; the corresponding final M/L would be around 25 for a stellar mass-to-light ratio of 5, in fairly good agreement with the observations (Mateo 1998) and comfortably higher than the lower limit obtained by Lake (1990) for galactic dwarf spheroidals. From the figure it is evident that both models LIs1 and LNc4s1 have outer star counts high enough to match the data (model LIs1 actually overestimates the observed star counts, but note that projection effects imply a scatter of a factor $\gtrsim$2 in the counts; see Fig. 2); on the contrary, the NFW models with higher concentrations cannot match the data, notwithstanding their fairly large discs (we recall that we adopted a spin parameter twice as large as the typical value in these latter models).

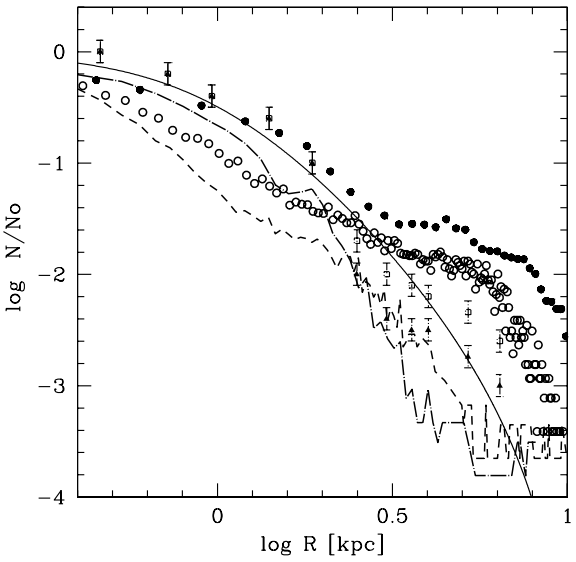

Figure 3. Projected star counts obtained for the remnants of model LIs1 (filled circles), model LNc4s1 (open circles), model LNc7s4 (dashed line) and model LNc12s4 (dot-dashed line), all with $V_c = 25$ km s^{-1}. Star counts are normalized to their value at the innermost radius (not shown because the plot is intended to cover mainly the outer region of the dwarfs). The line of sight is along one of the tidal tails and all the satellites are on the same orbit having $R_p = 75$ kpc and $R_{apo} = 230$ kpc. The squares with error bars are the number counts from Majewski et al. (2000) averaged over the four samples of giant stars, while the triangles are the same data corrected for a higher background contamination assuming a typical photometric error of 0.1 mag as in Morrison et al. (2001). A fit with a King profile with $c = 0.5$ (where $c = \log_{10}(r_t/r_c)$, r_t being the tidal radius and r_c being the core radius) is also shown (solid line).

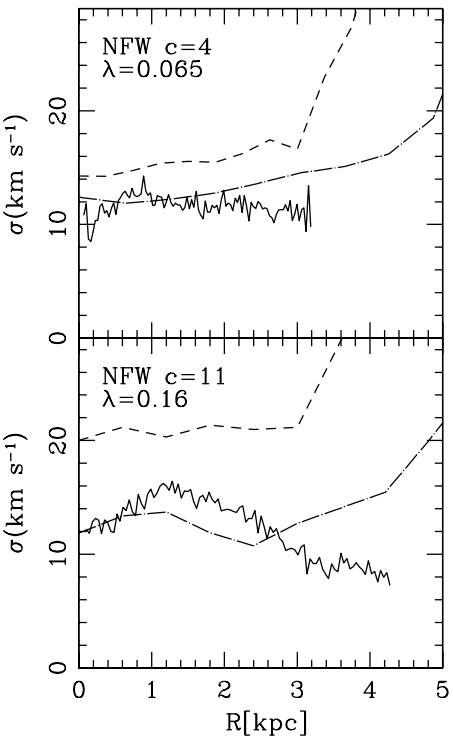

Figure 4. Intrinsic (solid line) versus apparent stellar velocity dispersion profiles for a line of sight along one of the tidal tails (dashed line) and for a line of sight, nearly perpendicular to the latter, that intercepts both tails (dot-dashed line). The models used in the simulations are LNc4s1 (upper panel) and the model with a highly concentrated halo and a large disc discussed in Section 4.1. The orbits have apo/peri = 2, with $R_p = 55$ kpc and both have haloes with an initial circular velocity $V_c = 25$ km s^{-1}.

The observational results of Majewski et al. (2000) have been questioned in Morrison et al. (2001), who show that their photometry is not accurate enough to distinguish between giant stars and dwarf stars (we note that spectroscopic confirmation of the giants is obtained in only a few cases). As a result, the number of giant stars might be overestimated by a factor ∼4. If this is the case, the counts close to the break radius would be brought down sensibly and a model with $c = 7$ might actually fit the data better than a model with $c = 4$ (see again Fig. 3). However, even in this case the observations cannot be matched by a galaxy having a halo with $c = 12$, a concentration comparable to or larger than this being expected in LCDM cosmogonies at the small mass scale considered here (Fig. 3).

In general, the presence of tidal extensions will lead to an overestimate in the velocity dispersions of the dwarf caused by unbound stars in projection; as already noted by others before (e.g. Piatek & Pryor 1995), a velocity gradient or an apparent rotation would also be observed as a result of the asymmetrical contamination introduced by tidal tails. Such apparent rotation would be observed when the line of sight intersects both tails. In our simulations, the apparent velocity dispersions in the central region of dwarfs are at most ∼40 per cent larger than the intrinsic maximum velocity dispersion, which would inflate the measured M/L by no more than a factor ∼2 (giving $M/L \lesssim 50$ in the remnants LNc4s1 and LIs1). This maximum enhancement occurs when the line of sight is aligned with one of the tails, so that a large amount of unbound, fast-moving stars are projected within the apparent boundaries of the dwarf. The enhancement is weaker when the line of sight intersects both tails; indeed, in order to separate the two tidal tails visually, the line of sight will be misaligned with both of them (these tend to point nearly towards the same direction, that of the orbital motion) and thus unbound stars will be scattered over a much larger area around the dwarf in this case. Fig. 4 illustrates how projection effects can alter the apparent kinematics but also shows that only measurements extending a few kiloparsecs from the centre would overestimate the intrinsic velocity dispersion significantly; therefore the contamination of kinematics induced by tails cannot explain the high mass-to-light ratios of dSphs without dark matter, contrary to previous claims (e.g. Kuhn & Miller 1989; Kuhn 1993).

Johnston et al. (1998) found that the contamination of streams in the projected star counts can show up even inside the intrinsic tidal radius of the satellites if the viewing angle is not perpendicular to the tails. We determined the final tidal radii of our remnants with the algorithm SKID, which identifies all the particles bound to the dwarf; we found that marginally bound particles are found as far as 3–4 kpc from the centre, namely at a larger distance than the break radius in any of the projections. However, this marginally bound region (which corresponds to the very inner part of the tails) comprises only a few per cent of the total mass of the remnant. We conclude that, although the break radius is not equivalent to the tidal radius, it roughly defines the boundary of the remnant, encompassing $\gtrsim$90 per cent of the bound mass.

3.2 Determining mass-loss rates using extratidal stars

Estimating the mass-loss rate of satellites from extratidal features is not a straightforward task. Johnston et al. (1998) have proposed a formula for estimating the mass-loss rate of an orbiting stellar

system which relies on the assumption that the number counts surface density profile of the extratidal material is $\Sigma_{\rm xt} \sim r^{-1}$. Majewski et al. (2000) have applied such a formula to the star counts profile they obtain for Carina and derive an extremely large fractional mass-loss rate, $\mathrm{d}f/\mathrm{d}t = 0.3$ Gyr^{-1}. This would imply that the mass of the stellar component in Carina would have been reduced by as much as a factor of 30 in 10 Gyr. We obtain comparable fractional mass-loss rates applying the same formula to the remnants in our simulations, while the actual average fractional mass-loss rates measured in the simulations (obtained by simply dividing the total mass lost by the duration of the simulation of about 10 Gyr) are significantly lower, $\sim$0.06 Gyr^{-1}.

One problem in applying the formula by Johnston et al. (1998) lies in the assumed radial surface density profile of the stream. In fact, the outer star counts profiles of our remnants are much flatter than r^{-1} for most of the viewing projections. Removing the constraint on the profile of the extratidal stars, Johnston et al. (1998) also derive an upper limit for the mass-loss rate:

$$\frac{\mathrm{d}f}{\mathrm{d}t} = \cos\theta \frac{\Sigma_{\rm xt}(r_{\rm break})}{n_{\rm break}} \frac{\pi}{T_{\rm orb}} 2\pi r_{\rm break}^2, \quad (1)$$

where θ is the angle between the velocity vector of the satellite and the line of sight (which can be derived for those satellites that have measured proper motions), $n_{\rm break}$ is the number of stars counted within $r_{\rm break}$ (the radius where the profile changes slope) and $T_{\rm orb}$ is the orbital time. Using equation (1) for the cases with clear tidal features we obtain $\mathrm{d}f/\mathrm{d}t < 0.5$ Gyr^{-1}, which, although correct, is not representative of the numerical results, being higher than the real mass-loss rate by nearly an order of magnitude.

Equation (1) is derived under the assumption that the stars are lost continuously over the orbital time $T_{\rm orb}$. However, the tidal mass loss for a satellite moving on an eccentric orbit will occur mostly as a result of the tidal shocks suffered at pericentre and will depend on its ability to respond to the perturbation and eventually adjust to a new equilibrium. To gain a better insight into the mechanism, we can consider a galaxy that suffers a few tidal shocks of duration $\tau = R_{\rm p}/V_{\rm p}$, where $R_{\rm p}$ and $V_{\rm p}$ are, respectively, the distance and the velocity of the galaxy at the pericentre of the orbit. On the apo/peri = 3 orbits often used in our simulations, $R_{\rm p} = 75$ kpc and $V_{\rm p} \sim 300$ km s^{-1}, hence $\tau \sim 2 \times 10^8$ yr. We also have $\tau \lesssim t_{\rm dyn}$, where $t_{\rm dyn}$ is the internal dynamical time of the satellites. We can calculate the heating of the stars due to the shocks using the 'extended' impulse approximation formulated by Gnedin & Ostriker (1997) and Gnedin, Hernquist & Ostriker (1999); the latter takes into account the adiabatic corrections needed when internal time-scales and shock duration are comparable (Weinberg 1994a,b,c). The characteristic time required for a star at the disc half-mass radius $r_{\rm hm}$ to increase its mean square velocity $\langle v^2 \rangle$ due to the shock is $t_{\rm shock} \sim (T_{\rm orb}/2)\sigma_\star^2/\langle \Delta v^2 \rangle$, where $\sigma_\star$ is the velocity dispersion of the stars [the factor of 2 accounts for the fact that two shocks occur during one orbital time; see Gnedin & Ostriker (1997)] and Δv is the impulse resulting from the shock. Typically satellites suffer three tidal shocks by the end of the simulations (see Fig. 5). We thus define also $t_{\rm heat} = t_{\rm shock}/3$ as the time-scale associated with the overall heating of the stars at the half-mass radius (corresponding to the total impulse $3\Delta v$); by doing this we neglect that the potential of the satellite, and thereby $\sigma_\star$, is evolving with time (the comparison with the simulations will show how limiting is such an assumption). This time-scale will be proportional to the mass-loss rate (see Binney & Tremaine 1987); in general, $t_{\rm heat}$ will be a lower limit to the time-scale over which the satellite loses 50 per cent of its initial disc mass (we recall that $t_{\rm shock}$ was defined at $r_{\rm hm}$) – indeed stars will have increased their kinetic energy substantially on such a time-scale but the system might expand and readjust to a new equilibrium before they can actually escape.

Gnedin et al. (1999) have provided analytical formulae to calculate $\langle \Delta v^2 \rangle$ for a satellite that is shocked by an extended perturber with an isothermal profile. As shown by these authors, if the orbits are eccentric, a good approximation is obtained by simply assuming that the satellite is moving on a straight path. In the latter case we can write

$$\langle \Delta v^2 \rangle = \left(\frac{GM_0}{R_{\rm p}^2 V_{\rm p}} \right)^2 \frac{r^2\pi^2}{3} \frac{R_{\rm p}^2}{R_{\rm max}^2} [1 + (\omega\tau)^2]^{-2.5}, \quad (2)$$

where M_0 and $R_{\rm max}$ are the total mass and radius of the perturber, and the last term in the product is the first-order adiabatic correction (ω is the typical stellar frequency at $r = r_{\rm hm}$, and $\omega\tau = \tau/t_{\rm dyn}$, where $t_{\rm dyn}$ is now the dynamical time at $r = r_{\rm hm}$). For a satellite with $V_{\rm c} = 25$ km s^{-1}, $\sigma_\star = V_{\rm c}/\sqrt{2}$, in either an isothermal halo or an NFW halo with $c = 4$ we have $r_{\rm hm} = 2$ kpc and $\omega\tau = \tau/t_{\rm dyn} \sim 1$; since $T_{\rm orb} \approx 2$ Gyr in our simulations, we obtain $t_{\rm heat} \sim 5.8$ Gyr. (Note that in models with higher c the adiabatic corrections will increase in magnitude.)

Fig. 5 shows that satellites on apo/peri = 3 orbits have lost about 40 per cent of their mass after 7 Gyr. As expected the actual mass loss appears slightly lower than predicted on the basis of $t_{\rm heat}$. None the less, the agreement is rather satisfactory because the complex time-dependent behaviour of the stellar potential, neglected by our estimate and related mainly to the non-axisymmetric instabilities, involves the mass distribution *inside* $r_{\rm hm}$ (bars have a radius $\sim r_{\rm h} < r_{\rm hm}$; see Mayer et al. (2001b). In the inner regions of the galaxies, the adiabatic corrections described above are more important and should be further increased as the stellar component becomes more concentrated as a result of bar formation; this will prolong the overall lifetime of the satellite beyond what one would infer by simply extrapolating our simple estimate of the characteristic mass-loss rate.

The resulting average fractional mass-loss rate is $\sim$0.1 Gyr^{-1}. The agreement with the simulations strongly depends on the adiabatic

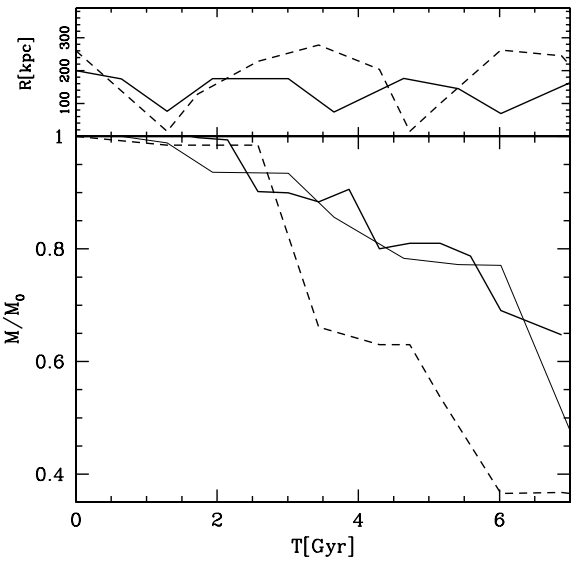

Figure 5. Fractional mass loss over 7 Gyr for satellites on an orbit with apo/peri = 3 and $R_{\rm p} = 75$ kpc (the thick solid line refers to model LIs1 and the thin solid line to model LNc4s1) and on an orbit with apo/peri = 15 and $R_{\rm p} = 20$ kpc (the dashed line, corresponding to model LIs1).

corrections; if we neglect them, the predicted mass-loss rate would be higher by a factor $\gtrsim$5 and would be closer to the predictions of Johnston et al. (1998).

Using the numerical results as a guide, we propose a simple recipe to infer the mass-loss rate from the observed star counts profile. On typical orbits like those considered here, the dwarfs lose mass at a rate that scales as $\sqrt{(N_s/N_0)}$. Employing the simulations that match the data on Carina to calibrate our estimate (these yield a fractional mass-loss rate $\mathrm{d}f/\mathrm{d}t \sim 0.6\ \mathrm{Gyr}^{-1}$), we obtain $\mathrm{d}f/\mathrm{d}t \sim 0.6\sqrt{(N_s/N_0)}\ \mathrm{Gyr}^{-1}$. This result was derived for the satellites on orbits with apo/peri = 3, but the mass-loss rates on nearly radial orbits differ by less than a factor of 2 (see Fig. 5). Calculating the mass loss in the same model but with projected profiles corresponding to different viewing angles also yields a scatter of a factor ~2.

3.3 Precession and heating of tidal streams

For dwarfs orbiting in spherical and smooth potentials like those considered so far, the escaping stars form symmetric tidal tails that lead and trail the satellite revealing its future and past orbit (see also Moore & Davis 1994). However, in general the orbital evolution of the streams will depend on the structure of the underlying potential and in turn the streams might be used as a tracer of such structure only provided that they remain sufficiently coherent (Johnston et al. 1999; Zhao et al. 1999). Cold dark matter haloes are complex triaxial systems with shapes and angular momenta that vary considerably from the centre to their virial radii (Moore et al. 2001; Jing & Suto 2002). They also contain dark matter substructure and satellite galaxies that can heat and perturb parts of the stream away from their orbital paths. These effects might combine to destroy the coherent nature of tidal streams through differential precession of orbits (see also Johnston, Sackett & Bullock 2001).

To investigate the long-term evolution of tidal tails, we first construct a massless spherical system using 50 000 particles distributed with a density profile $\rho(r) \propto r^{-1}$, radius 10 kpc and velocity dispersion $\sigma_{1\mathrm{d}} = 10\ \mathrm{km\ s}^{-1}$. This unbound test satellite will form tidal streams that can be used to explore orbits within different haloes. The evolution of this system on a series of circular orbits within a smooth spherical potential is shown in Fig. 6. This potential is a dark matter halo with density profile $\rho(r) \propto r^{-2}$ and constant velocity dispersion $\sigma_{\mathrm{halo}} = 220/\sqrt{2}\ \mathrm{km\ s}^{-1}$, i.e. the same Milky Way halo model used in the previous sections. The rings of debris correspond to satellites on initially circular orbits at radii of 0.2, 0.4, 0.6, 0.8 and 1.0 R_{200} where $R_{200} = 300$ kpc.

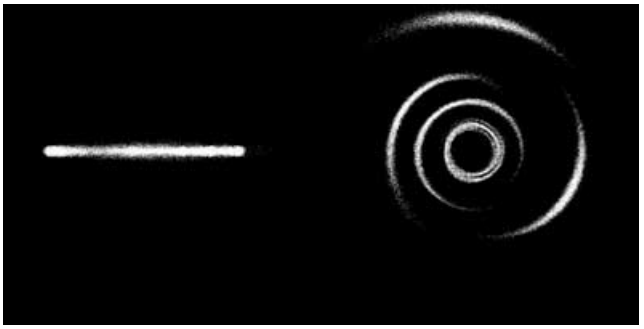

Figure 6. The evolution of five massless satellites on circular orbits within a smooth spherical potential for a period of 6 Gyr (comparable to the orbital time of the outer satellite). On the left is an edge-on view of the orbital plane and on the right is a face-on view.

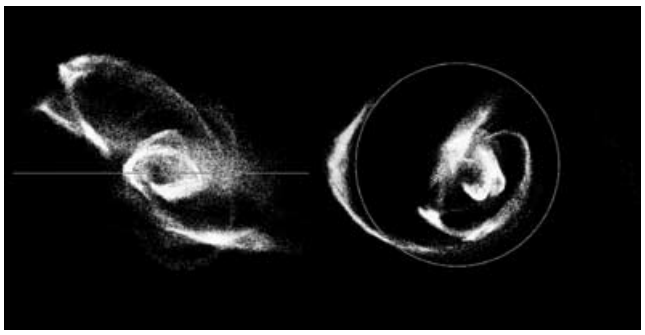

Figure 7. The evolution of five massless satellites on initially circular orbits (same as in Fig. 6) within a CDM galactic mass halo. The satellites are introduced at a redshift $z = 0.5$ and the simulation is continued to the present day. On the left is an edge-on view of the initial orbital plane and on the right is a face-on view.

The unbound satellite immediately starts to form symmetric tidal tails. The tidal debris lies in the orbital plane, and after a time-scale of 6 Gyr the particles lie in streams that wrap around more than one orbit at the centre of the potential and about 10 per cent of an orbital radius at the edge.

We now repeat the test using a CDM halo taken from one of the cosmological simulations of Moore et al. (1999a). By construction, the circular velocity and virial radius are similar to those adopted in the spherical potential above. The halo is resolved with 10^6 particles within R_{200} and we use a comoving softening length of 0.5 kpc. This particular galactic mass halo virializes by a redshift $z = 0.5$ and does not accrete any bound object containing more than 1 per cent of its mass by the present day. We calculate the axis with the largest component of angular momentum and place the test satellites on circular orbits at the same radii as used in the spherical potential above.

Fig. 7 shows the satellite particles after a period of ~6 Gyr, revealing that the tidal streams have precessed dramatically away from their initial orbits. The inner streams have wrapped several times around the halo, both within and out of the orbital plane, whilst the outer streams remain more coherent but have precessed from their initial orbital plane by over 45°. The precession induced by the differentially rotating triaxial halo and eventually by perturbing lumps is mostly responsible for the differences between the orbits of the tidal debris between Figs 6 and 7. However, the substructure in the galactic CDM halo has also contributed visible tidal heating to the streams. This is most noticeable in the outer streams, which have a clumpy appearance due to heating by the most massive subhaloes. Indeed, dark matter substructure in the outer halo will be more massive because dynamical friction times and tidal disruption times are both longer there (Colpi, Mayer & Governato 1999) and will cause the most heating.

Numerical heating of the streams due to massive halo particles (Moore et al. 1996) might somewhat enhance the observed evolution of the streams. In order to test our results, we ran a massless spherical satellite in a 10^5 particles Milky Way-sized halo with an NFW profile; this halo is similar to the CDM halo as far as mass distribution and size are concerned, but it is spherical and smooth (no substructure), and therefore no physical heating or precession is expected. After 10 Gyr we measured fluctuations of only a few per cent in the orbital energy and orbital angular momentum, and, correspondingly, the initial orbital plane of the satellite is barely

altered. This shows that two-body heating has a negligible contribution to the evolution of the streams (this is a conservative test since the CDM halo in the cosmological volume had a resolution almost 10 times higher). Clearly, this test focuses only on the effect of two-body heating by particles in the primary halo, while heating by substructure itself might also depend on resolution: indeed subhaloes are expected to be denser and survive longer with increasing resolution, eventually perturbing the streams more through more and more effective collisions (Moore et al. 1996). Therefore the simulations adopting the CDM halo actually provide a lower limit to the effect of substructure.

One would like to disentangle the role of halo shape from that of substructure in the dynamical evolution of streams within the CDM halo. Precession of streams originating from satellites orbiting close in the inner Milky Way halo should happen very fast, on a scale comparable to the orbital time, even in smooth, moderately triaxial systems. In the simple case of a spheroidal halo with an axial ratio of $q = 0.75$, a stream on a nearly circular orbit at 30 kpc from the centre that is neither polar nor in the equatorial plane can precess by 60° in 1 Gyr (Ibata et al. 2001a). We ran a few more tests using the usual spherical massless satellites on orbits with radii either 0.2 or $0.8R_{200}$ in a flattened, isothermal Milky Way halo with $q = 0.75$ and compared the results with those obtained before within a spherical Milky Way halo [the flattened model is the same Dehnen & Binney (1998) model used in Ibata et al. (2001a), except that we omit the exponential truncation at large radii because it was not present in the spherical mode]. In Fig. 8 we show streams of satellites originally placed on orbits with different radii or in haloes with different shapes; as can be seen, precession after 6 Gyr is dramatic on inner orbits, while it is fairly moderate, around 30°, on outer orbits. The amount of precession observed in these tests is comparable to that occurring for satellites on similar orbits in the CDM halo, being only slightly smaller for satellites on outer orbits (we caution that orbital dynamics are more complex in the CDM halo, which is triaxial as opposed to axisymmetric). Therefore, we conclude that the precession in the latter must be caused more by the non-spherical halo shape than by the perturbing lumps. However, the substructure will also affect the spatial distribution of the streams by tidally heating them through encounters.

The experiments illustrated so far have adopted massless satellites that are immediately disrupted; more realistic satellites, like those considered in the previous sections, lose mass more gradually and mostly close to pericentre. Stars lost at different times would trace different orbits and would have precessed by a different degree at a given time; this is what actually causes the stream in a flattened halo to appear less coherent than in a spherical halo when observed projected on to the plane of the sky as in Ibata et al. (2001a). This is illustrated in Fig. 9; the streams shown originate from satellites that were placed on the same orbits and in the same haloes as those displayed in Fig. 8, but this time the satellites have non-zero mass (their mass corresponds to a circular velocity $V_c = 50$ km s^{-1} and the corresponding velocity dispersion is $\sigma = V_c/\sqrt{2} \sim 35$ km s^{-1}). In general, streams escaping satellites of a given mass mass will be more or less spread out depending on the velocity dispersion and radius of the satellite. However, as both quantities scale as $M^{1/3}$ in CDM models, this is equivalent to saying that more massive satellites will lead to streams distributed on a larger volume in phase space in these cosmogonies.

In our analysis we have ignored the dissipative effects of a baryonic component that could help regularize the structure of the inner dark matter halo. However, the outer halo would remain unaffected by the adiabatic contraction and this tends to produce oblate inner haloes (Dubinski & Carlberg 1991). Coherent streams should only be found in the equatorial plane or on polar orbits.

Figure 8. Streams of a massless satellite (see text) after 6 Gyr viewed along the initial orbital plane. From top to bottom: circular orbit with $r = 0.2R_{200}$ in a spherical halo; circular orbit with $r = 0.2R_{200}$ in a halo with $q = 0.75$; and circular orbit with $r = 0.8R_{200}$ in a halo with $q = 0.75$.

Our results suggest that evidence of streams associated with narrow regions or strips in galaxy and cluster haloes would support models in which the dark matter behaves like a fluid. In this case, haloes are highly spherical and contain less mass attached to subhaloes due to ram-pressure stripping (Peebles 2000). Interestingly, the stream associated with the Sagittarius dwarf spheroidal is a great

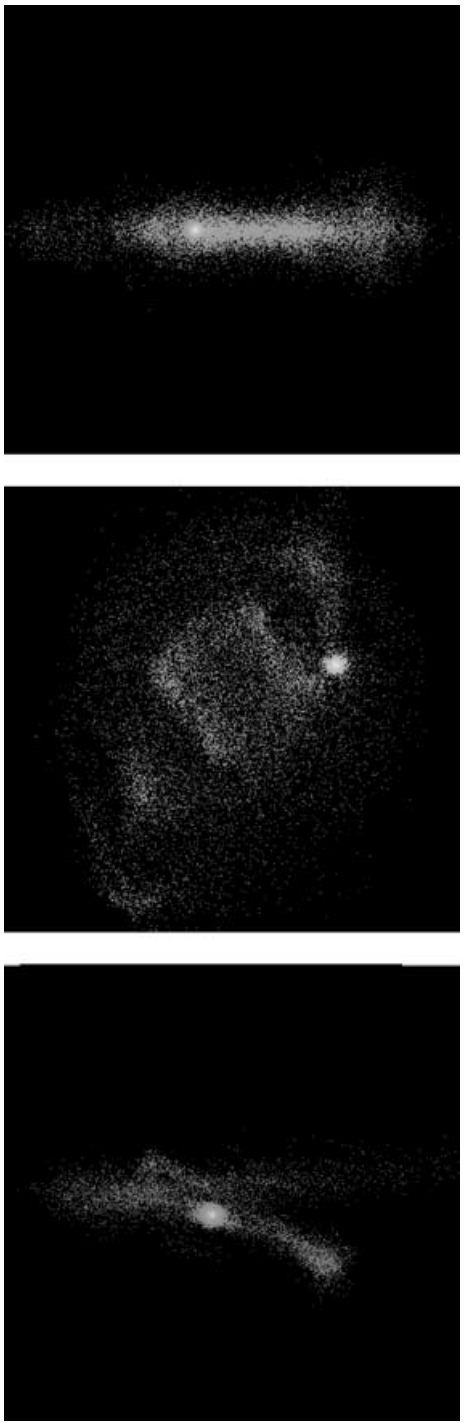

Figure 9. Streams of a satellite with initial mass of 10^{10} $M_\odot$ (see text) after 6 Gyr viewed along the initial orbital plane. From top to bottom: circular orbit with $r = 0.2R_{200}$ in a spherical halo; circular orbit with $r = 0.2R_{200}$ in a halo with $q = 0.75$; and circular orbit with $r = 0.8R_{200}$ in a halo with $q = 0.75$.

circle according to Ibata et al. (2001a). These authors use carbon stars distributed through a large portion of both the southern and the northern sky as a tracer of the stream and have recently argued that the Galactic halo must be nearly spherical between 16 and 60 kpc from the centre. Other authors might have identified the northern tip of the same stream using A-type stars (Yanni et al. 2000) and RR Lyrae stars (Ivezic et al. 2000) from the Sloan Digital Sky Survey (SDSS). More recently, Martinez-Delgado et al. (2001b) identify a low-density stellar system in the same region and conclude that it could be either the northern stream of the Sagittarius dwarf spheroidal or a stream associated with another dwarf galaxy. We note that both the field of the SDSS and that used by Martinez-Delgado et al. (2001b) are too small to allow a determination of the actual spatial extent of the stream. The confirmation that these detections are actually related to the Sagittarius stream or to the streams of other disrupted satellites will allow a new test to structure formation models.

The evolution of the streams in the smooth, non-spherical halo used in some of our experiments is quite similar to that in the lumpy CDM halo. Hence streams in a mildly lumpy but still triaxial WDM halo (Bullock 2001, Governato et al., in preparation) would probably look similar to those in a CDM halo and would be equally hard to interpret observationally. The outer part of the halo, where the perturbations induced by substructure significantly contribute to alter the spatial distribution of the streams, will be the one to target in order to find evidence of a smoother potential. On the other hand, the most massive satellites will cause the most heating, and these would be present in CDM models as well as in plausible WDM models (Barkana, Haiman & Ostriker 2001; Knebe et al. 2002). We intend to analyse in detail the evolution of streams in WDM haloes versus CDM haloes in a forthcoming paper, where we will also quantify the dynamical effect of substructure in different regions of the halo.

4 DISCUSSION

In the first part of this paper we have shown that the outer flattening observed in the stellar profiles of some dSphs can provide a constraint on the structure of their dark matter haloes once their orbital eccentricity is known. At present, the few proper motions available [e.g. Kroupa & Bastian (1997) for the Large and Small Magellanic Clouds (LMC and SMC), Schweitzer et al. (1995) for Sculptor and Schweitzer & Cudworth (1996) for Ursa Minor] imply that the Galactic satellites have orbits with low eccentricities, corresponding to typical apo/peri = 2–3. It is clear that systems on these orbits with concentrations as high as predicted in the standard LCDM cosmology (Eke et al. 2001) for galaxies with $V_c < 50$ km s^{-1} ($c \geqslant 10$) would not be able to reproduce the observed star counts of the Carina dSph (see Fig. 3). This is true even if the outer number counts are reduced based on the typical photometric errors estimated in Morrison et al. (2001). The only chance to bring data into agreement with the numerical results at high halo concentrations would be lowering the counts further by more than a factor of 5. Clearly future observations will have to assess better the shape of the surface brightness profiles of Carina and other dwarfs and obtain accurate measurements of the kinematics out to large radii. Only a combination of very accurate star counts and velocity dispersion profiles will allow one to establish firmly the existence of tidal tails (whatever the projection, velocity dispersion has to rise at outer radii if tails are present, see Fig. 4) and draw robust conclusions on halo structure from them.

When interpreting our results in the context of structure formation, we need to take into account that the properties of haloes in CDM models have some scatter, mainly because there is a spread in formation times for a given mass scale (Navarro et al. 1997). However, recently Bullock et al. (2001) have measured the scatter of the concentration of halo profiles in LCDM simulations and, according to their results, a concentration of $c = 7$ is too low for haloes with $M \sim 10^{11}$ $M_\odot$, while a concentration of $c = 12$ would be close to the lower limit at the same mass scale. The mass scale of $\sim 10^{11}$ $M_\odot$

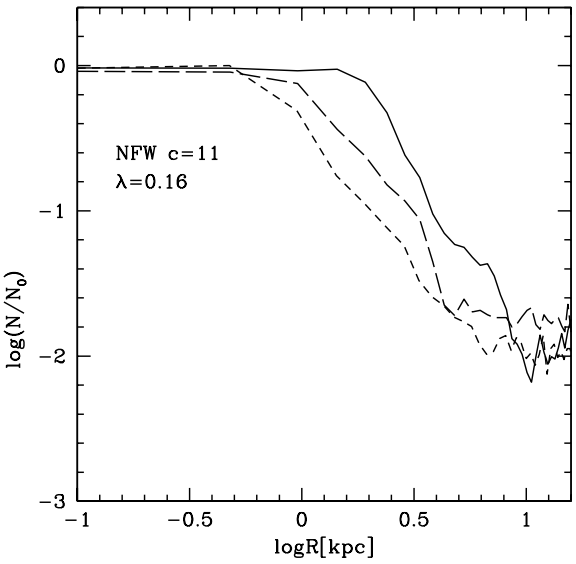

Figure 10. Projected star counts for the remnant (after 7 Gyr) of a satellite model with a highly concentrated halo. The satellite has $V_c = 25$ km s^{-1} and was placed on an orbit with apo/peri = 2 and $R_p = 55$ kpc. We show the projected star counts along one of the tails (solid line) and along the two lines of sight perpendicular to the former (short dashed and long dashed lines).

corresponds to the most massive among the models considered in this paper. The models whose remnants fit better the observed properties are more than 10 times lighter and thus should have higher minimum concentrations. No cosmological simulations are available yet that statistically probe such small scales, but Bullock et al. (2001) show that the dependence of mass on concentration goes as $M^{-0.13}$. Even if such a dependence is much shallower than that originally proposed by Navarro et al. (1996), it still yields an increase of a factor ∼1.5 in concentration over an order of magnitude in mass, suggesting that we are being conservative in our comparisons.

Satellites with either softened isothermal haloes or cuspy haloes with low concentrations exhibit features that can reproduce the observations – even on orbits with moderate eccentricities. Interestingly we note that the low values of the concentration needed ($c < 5$) are found in WDM models at the dwarf galaxy scale (Eke et al. 2001; Avila-Reese et al. 2001).

4.1 High mass-to-light ratios in dSphs

Our results have implications on the actual dark matter content of dSphs. Large tidal tails are produced only when the dark matter in the remnants accounts for $\leqslant$80 per cent of the total mass. The apparent M/L can be at most twice the intrinsic value because of the unbound stars projected along the line of sight, and therefore we expect to find tidal tails only around dwarfs whose measured M/L is not very high. Indeed most of the dSphs in the Local Group, including Carina, have $M/L \leqslant 30$ (Mateo 1998).

The dark matter contents of Draco and Ursa Minor, with $M/L > 60$ (Hargreaves et al. 1994a,b; Mateo 1998), are instead too high even accounting for enhanced apparent velocity dispersions. Such high dark matter contents would be incompatible with the observations of massive tails; the remnants that have similarly large dark matter contents at the end of our simulations [see also Mayer et al. (2001a,b) on the evolution of the GR8 model] have star counts at the level $N_s/N_0 < 10^{-3}$ in the outer part. Although very recent results exclude the presence of tails in Draco (Odenkirchen et al. 2001; Aparicio, Carrera & Martinez-Delgado 2001), other authors have reported positive detections of some extratidal stars around the latter dwarf and Ursa Minor (Piatek et al. 2001; Martinez-Delgado et al. 2001b).

In order to explore this issue further, we ran a simulation with a satellite model different from those used so far. We used an NFW halo with a high concentration, $c = 11$, and $V_c = 25$ km s^{-1}, and a disc extending out to half of the virial radius of the halo, ≈10 kpc, corresponding to a very high spin parameter, $\lambda = 0.16$, and a very low central surface brightness, $\mu_B \sim 25$ mag arcsec^{-2}. We placed the model on an orbit with an apo/peri = 2 and a pericentre $R_p =$ 55 kpc, consistent with the present distances and radial velocities of Draco and Ursa Minor (Mateo 1998). After 7 Gyr the satellite has turned into a dSph ($v_{rot}/\sigma \sim 0.3$) with a central velocity dispersion $\sigma \sim 10$ km s^{-1} and a dark matter halo still seven times more massive than the stellar component; this would yield $M/L > 40$ for a stellar mass-to-light ratio ∼5 (Mayer et al. 2001b). Furthermore, owing to its unusually large scalelength, the stellar component has undergone severe stripping, producing prominent tidal tails and signatures in the star count profile qualitatively similar to those observed in Carina (Fig. 10); including possible projection effects due to the tidal tails, the apparent mass-to-light ratio could be enhanced up to values around 80. This experiment shows that an extremely extended disc can produce large tails notwithstanding the high central dark matter density of the halo. How realistic is such an experiment? A closer look shows that the remnant is very extended in radius and the flattening of the star counts in the remnants occurs at more than 4 kpc, which is too far out compared to the size of Draco, the latter being less than 1 kpc (Mateo 1998). In addition, a dwarf progenitor with an extremely extended disc is hard to support from the observational point of view. The rotation curves of dIrrs and LSB spirals suggest that the scalelengths of haloes and baryons are correlated (de Blok & McGaugh 1997) and in some cases the scalelength of the halo can be larger than the typical disc size (Lake 1990), while in the present model it is considerably smaller. Most importantly, the surface density of the gas in the outer part of such an extended disc would be so low that the star formation would have hardly occurred, making the issue of stellar tail formation rather pointless.

The correct evaluation of the M/L of dSphs is important when one tries to compare the observed number of Galactic satellites with the numbers predicted by cosmological *N*-body simulations (Moore et al. 1999a; Klypin et al. 1999). It has been pointed out that dwarfs with NFW haloes should have rising velocity dispersion profiles and that by using the measured *central* velocity dispersions one would actually underestimate the total mass of dSphs; including this correction would improve the agreement with observations (Moore 2001). As for this issue, our simulations suggest two possible scenarios based on results such as those shown in Fig. 4. First, if it were confirmed that most of the satellites have large tidal tails and that their orbits have low eccentricity, then it is very likely that their haloes have low concentrations, $c < 10$, and have quite flat intrinsic and apparent velocity dispersion profiles (Fig. 4, upper panel). The apparent velocity dispersion can actually be higher than any value of the intrinsic velocity dispersion, but never smaller, which would actually tend to *reverse* the correction. Secondly, even if the satellites had more concentrated NFW haloes, (1) the intrinsic peak velocity dispersion is only ∼25 per cent higher than the central value in the remnants, and (2) if significant tidal tails are present, because of very eccentric orbits or unusually large discs, the intervening stellar debris tends again to both raise and flatten the apparent velocity dispersion profile (see Fig. 4, lower panel). Hence, it seems that a better assessment of the actual mass of the dwarfs derived from

apparent velocity dispersions would hardly alleviate the substructure problem and could actually make it worse.

5 SUMMARY

We have used numerical simulations of two component models of dwarf galaxies orbiting within a Milky Way potential to study the effects related to their tidal tails. The signatures produced by the tidal debris in the stellar profiles can be used to constrain the structure of the dark matter haloes of dwarfs, providing hints to the nature of the dark matter. The long-term evolution of tidal debris was followed within a smooth, spherical and flattened potential and within a high-resolution cold dark matter halo. We summarize our conclusions here:

(i) We can produce tails as prominent as those observed around the Carina dSph with models having soft central potentials, while with models having highly concentrated potentials the same observations can be matched only on nearly radial orbits. Hence knowledge of the orbits of the dSphs is vital to constrain directly their internal structure. If it is confirmed that the orbits are nearly circular, warm dark matter models will be favoured instead of cold dark matter.

(ii) Models with very high mass-to-light ratios and strong tidal tails are very difficult to produce. Draco and Ursa Minor should only have very weak tails, at a star count level at least 10 times lower than that found in Carina. Their inner structure might be consistent with the predictions of CDM models, but could be easily reproduced even with softer halo potentials provided that the stellar component has a scalelength as small as that of some of the faintest dwarf irregulars found in the Local Group [as in model LIs3 of this paper or in the 'GR8' model in Mayer et al. (2001b)].

(iii) Our simulations provide a simple estimate of the mass-loss rates of dSphs based on star counts and these are significantly lower than those obtained in other works that discarded adiabatic corrections; Carina is likely to survive for at least another 5 Gyr.

(iv) Only satellites on very tightly bound orbits, like Sagittarius, which suffered many strong tidal shocks, could have already been destroyed in the past or could now be close to disruption.

(v) The masses of dwarf spheroidals could be overestimated when large tidal tails are present but the maximum effect due to projection of unbound stars is only a factor of 2. However, this would shift the mass function of galactic satellites further away from that predicted by cold dark matter models, making the substructure problem even worse.

(vi) The tidal debris within a CDM halo shows dramatic signatures of differential precession and heating by dark matter substructures. Precession is mostly caused by the non-spherical shape of CDM haloes and is the main driver of the loss of coherence of the streams on inner orbits. Heating by substructure is instead more important for satellites on outer orbits. It may be impossible to use observations of tidal streams to map the structure of the Galactic halo if the latter is substantially non-spherical and lumpy as predicted by CDM cosmogonies.

(vii) If many examples of coherent tidal streams are discovered, then this would favour fluid dark matter models, which produce smoother and highly spherical dark matter haloes. Therefore, observations of tidal streams can be used to probe the nature of dark matter. However, further analysis is required to investigate whether it would be possible to distinguish between triaxial haloes with a different degree of lumpiness, like CDM and WDM haloes.

ACKNOWLEDGMENTS

We thank the anonymous referee for helpful comments and suggestions. The simulations were performed on the ORIGIN 3800 at the CINECA Supercomputing Centre in Bologna and on an ALPHA workstation at the University of Washington. LM thanks Volker Springel for providing the code used to construct the galaxy models and Elena d'Onghia for providing the algorithm to fit King profiles to the simulations. LM was supported by the National Science Foundation (NSF Grant 9973209).

REFERENCES

Aparicio A., Carrera R., Martinez-Delgado D., 2001, AJ, 122, 2524
Avila-Reese V., Colin P., Valenzuela O., D'Onghia E., Firmani C., 2001, ApJ, 559, 516
Barkana R., Haiman Z., Ostriker J. P., 2001, ApJ, 558, 482
Barnes J., Efstathiou G., 1987, ApJ, 319, 575
Binney J., Tremaine S., 1987, Galactic Dynamics. Princeton Univ. Press, Princeton, NJ
Bode P., Ostriker J., Turok N., 2001, ApJ, 556, 93
Bottema R., 1997, A&A, 328, 517
Bullock J. S., 2001, Proc. Workshop on The Shapes of Galaxies and Their Halos, Yale Univ. (astro-ph/0106380)
Bullock J. S., Kolatt T. S., Sigad Y., Somerville R. S., Kravtsov A. V., Klypin A. A., Primack J. R., Dekel A., 2001, MNRAS, 321, 559
Colpi M., Mayer L., Governato F., 1999, ApJ, 525, 720
Cote S., Freeman K. C., Carignan C., 1997, in Persic M., Salucci P., eds, ASP Conf. Ser. Vol. 117, Dark and Visible Matter In Galaxies. Astron. Soc. Pac., San Francisco, p. 52
Dalcanton J. F., Hogan C. J., 2001, ApJ, 561, 35
de Blok W. J. G., McGaugh S. S., 1997, MNRAS, 290, 533
de Blok W. J. G., McGaugh S. S., Bosma A., Rubin V. C., 2001, ApJ, 552, L23
Dehnen W., Binney J. J., 1998, MNRAS, 294, 429
Dikaiakos M., Stadel J., 1996, Proc. Int. Conf. on Supercomputing. Assoc. for Computing Machinery, New York
Dohm-Palmer R. C. et al., 2001, ApJ, 555, L37
Dubinski J., Carlberg R., 1991, ApJ, 478, 496
Dubinski J., Mihos C., Hernquist L., 1996, ApJ, 462, 576
Eke V. R., Navarro J. F., Steinmetz M., 2001, ApJ, 554, 114
Fall S. M., Efstathiou G., 1980, MNRAS, 193, 189
Firmani C., D'Onghia E., Avila-Reese V., Chincarini G., Hernandez X., 2000, MNRAS, 315, L29
Gardner J. P., 2001, ApJ, 557, 616
Ghigna S., Moore B., Governato F., Lake G., Quinn T., Stadel J., 2000, ApJ, 544, 616
Gnedin O. Y., Ostriker J., 1997, ApJ, 474, 223
Gnedin O. Y., Hernquist L., Ostriker J., 1999, ApJ, 514, 109
Grebel E. K., 1999, in Whitelock P., Cannon R., eds, Proc. IAU Symp. 192, The Stellar Content of Local Group Galaxies. Astron. Soc. Pac., San Francisco, p. 17
Grebel E. K., 2001, Ap&SS, 277, 231
Haiman Z., Thoul A., Loeb A., 1996a, ApJ, 464, 523
Haiman Z., Rees M., Loeb A., 1996b, ApJ, 467, 522
Hargreaves J. C., Gilmore G., Irwin M. J., Carter D., 1994a, MNRAS, 269, 957
Hargreaves J. C., Gilmore G., Irwin M. J., Carter D., 1994b, MNRAS, 271, 693
Helmi A., White S. D. M., 1999, MNRAS, 302, 53
Helmi A., White S. D. M., de Zeeuw P., Zhao H., 1999, Nat, 402, 53
Hernquist L., 1993, ApJS, 86, 289
Ibata R. A., Lewis G. F., 1998, ApJ, 500, 575
Ibata R. A., Lewis G. F., Irwin M., Totten E., Quinn T., 2001a, ApJ, 551, 295
Ibata R. A., Irwin M., Lewis G., Ferguson A., Tanvir N., 2001b, Nat, 6842, 49

Irwin M., Hatzidimitriou D., 1995, MNRAS, 277, 1354
Ivezic Z. et al., 2000, AJ, 120, 963
Jing Y. P., Suto Y., 2000, ApJ, 503, L9
Jing Y. P., Suto Y., 2002, ApJ, 574, 538
Johnston K. V., Sigurdsson S., Hernquist L., 1998, MNRAS, 301, 771
Johnston K. V., Zhao H., Spergel D. N., Hernquist L., 1999, ApJ, 512, L109
Johnston K. V., Sackett P. D., Bullock J., 2001, ApJ, 557, 137
Klessen R., Kroupa R., 1998, ApJ, 498, 143
Klypin A., Kravtsov A. V., Valenzuela O., Prada F., 1999, ApJ, 522, 8
Knebe A., Devriendt J. E. G., Mahamood A., Silk J., 2002, MNRAS, 329, 813
Kroupa P., Bastian U., 1997, New Astron., 2, 139
Kuhn J. R., 1993, ApJ, 409, L13
Kuhn J. R., Miller R. H., 1989, ApJ, 341, L41
Lake G., 1990, MNRAS, 244, 701
Lake G., Skillman E. D., 1989, AJ, 98, 1274
McGaugh S., Rubin V., de Blok E., 2001, AJ, 122, 238
Majewski S. R., Ostheimer J. C., Patterson R. J., Kunkel W. E., Johnston K. V., Geisler D., 2000, AJ, 119, 760
Martinez-Delgado D., Alonso-Garcia J., Aparicio A., Gomez-Flechoso M. A., 2001a, ApJ, 549, L63
Martinez-Delgado D., Aparicio A., Gomez-Flechoso M. A., Carrera R., 2001b, ApJ, 549, L199
Mateo M., 1998, ARA&A, 36, 435
Mayer L., Governato F., Colpi M., Moore B., Quinn T., Wadsley J., Stadel J., Lake G., 2001a, ApJ, 547, L123
Mayer L., Governato F., Colpi M., Moore B., Quinn T., Wadsley J., Stadel J., Lake G., 2001b, ApJ, 559, 754
Mihos C., Dubinski J., Hernquist L., 1998, ApJ, 502, 141
Mo H. J., Mao S., White S. D. M., 1998, MNRAS, 296, 847
Moore B., 2001, in Wheeler J. C., Martel H., eds, Proc. Am. Inst. Phys. Conf. Vol. 586 Proc. 20th Texas Symp. AIP, New York, p. 73
Moore B., Davis M., 1994, MNRAS, 270, 209
Moore B., Katz N., Lake G., 1996, ApJ, 457, 455
Moore B., Ghigna S., Governato F., Lake G., Quinn T., Stadel J., Tozzi P., 1999a, ApJ, 524, L19
Moore B., Quinn T., Governato F., Stadel J., Lake G., 1999b, MNRAS, 310, 1147
Moore B., Gelato S., Jenkins A., Pearce F. R., Quilis V., 2000, ApJ, 535, L21
Moore B., Calcaneo-Roldan C., Stadel J., Quinn T., Lake G., Ghigna S., Governato F., 2001, Phys. Rev. D, 64, 063508
Morrison H. L., Olszewski E. W., Mateo M., Norris J. E., Dohm-Palmer R. C., Freeman K. C., 2001, AJ, 121, 283
Navarro J. F., Frenk C. S., White S. D. M., 1996, MNRAS, 275, 56
Navarro J. F., Frenk C. S., White S. D. M., 1997, MNRAS, 290, 493
Odenkirchen M. et al., 2001, ApJ, 122, 2538
Peebles P. J. E., 2000, ApJ, 534, L127
Peebles P. J. E., Vilenkin A., 1999, Phys. Rev. D, 60, 103506
Piatek S., Pryor C., 1995, AJ, 109, 1071
Piatek S., Pryor C., Armandroff T. E., Olszewski E. W., 2001, AJ, 121, 841
Power C., Navarro J. F., Jenkins A., Frenk C. S., White S. D. M., Springel V., Stadel J., Quinn T., 2002, MNRAS, submitted (astro-ph/0201544)
Schweitzer A. E., Cudworth K. M., 1996, in American Astronomical Society Meeting, 188, 09.01
Schweitzer A. E., Cudworth K. M., Majewski S. R., Suntzeff N. B., 1995, AJ, 110, 2747
Spergel D. N., Steinhardt P. J., 2000, Phys. Rev. Lett., 84, 3760
Springel V., White S. D. M., 1999, MNRAS, 307, 162
Tegmark M., Silk J., Rees M., Blanchard A., Abel T., Palla F., 1997, ApJ, 474, 1
Toomre A., Toomre J., 1972, ApJ, 178, 623
van den Bosch F. C., Robertson B. E., Dalcanton J., de Blok W. J. G., 2000, AJ, 119, 1579
Vivas A. K. et al., 2001, ApJ, 554, L33
Warren M. S., Quinn P. J., Salmon J. K., Zurek W. H., 1992, ApJ, 399, 40
Weinberg M. D., 1994a, AJ, 108, 1398
Weinberg M. D., 1994b, AJ, 108, 1403
Weinberg M. D., 1994c, AJ, 108, 1414
White S. D. M., Frenk C. S., 1991, ApJ, 379, 52
Yanni B. et al., 2000, ApJ, 540, 825
Yoshida N., Springel V., White S. D. M., Tormen B., 2000a, ApJ, 535, L103
Yoshida N., Springel V., White S. D. M., Tormen B., 2000b, ApJ, 544, L87
Zhao H., Johnston K. V., Hernquist L., Spergel D. N., 1999, A&A, 348, L49

This paper has been typeset from a TEX/LATEX file prepared by the author.